Detached Eddy Simulation of Base Flows under Subsonic Free Stream Conditions

By Y. You, H. Lüdeke, AND V. Hannemann

Institute of Aerodynamics and Flow Technology, German Aerospace Center (DLR)
Lilienthalplatz 7, 38108 Braunschweig
Bunsenstraße 10, 37073 Göttingen

The present work focuses on the numerical simulation of a base flow around a generic rocket model for subsonic flow conditions. In a preliminary study the flow for two reduced geometries are investigated to obtain an optimized discretization of the flow field for a detached eddy simulation (DES). First, an inflow plane with prescribed values from a Reynolds averaged Navier-Stokes (RANS) solution is used which avoids the unsteady simulation of the model support and most of the model body. Second, the problem size is halved by exploiting the symmetry of the geometry. In both calculations an indicator is tested, which quantifies the local grid quality with respect to the turbulent kinetic energy resolved by the DES. According to this indicator the grid resolution in the first case is very good and in the second case sufficient in the regions of interest. Although the physical interpretation is limited due to the approximations made, the results indicate a strong connection between the base flow and the wake of the support.

1. Introduction

The simulation of the unsteady base flow in the wake of launch vehicles, including separation, reattachment and turbulent shear phenomena plays an important role in the design and optimization process of such vehicles. It has been commonly accepted that the unsteadiness of afterbody flow can result in strong structural loads at low frequency, which endanger the structure of the launcher [1]. To reach a better understanding of the unsteady characteristics of such flows, a collaboration has been established under the national research program *Technological foundations for the design of thermally and mechanically highly loaded components of future space transportation systems (TR40).* While other working groups focus on the experiments and highly accurate numerical methods such as Large Eddy Simulation (LES), our group uses less accurate but faster numerical approaches. After investigating the limits of RANS solutions for the wake flow field [2], the study of generic base flows turns to Detached Eddy Simulations (DES), as a higher level of numerical complexity.

As the most common hybrid RANS/LES approach, DES has been extensively applied to study afterbody flows. For example Lüdeke and Deck studied the fluid structure interaction in the nozzle section of the Ariane 5 under transonic wind tunnel conditions [1, 3, 4]. The rich modal response of the nozzle shape on the unsteady flow field was investigated and a strong influence on the surface pressure distribution was shown in detail. Deck used both DES and LES to investigate the detailed flow features behind an axisymmetrical afterbody [4]. The computations were able to recover the predominant frequency at a Strouhal number of 0.2. Moreover, the jet suction effect on the

M_∞	$u_\infty\,[m/s]$	$Re_m\,[m^{-1}]$	$P_\infty\,[Pa]$	$T_\infty\,[K]$
0.2	70	4×10^6	10^5	315.65

TABLE 1. Experimental free stream flow conditions in the subsonic RWTH Aachen wind tunnel

base pressure distribution is well predicted in the paper. Beyond these investigations, Weiss and Deck also studied the flow control problem of a turbulent three dimensional axisymmetric step by means of continuous jets [5]. According to the DES results, they concluded that the rise of the three-dimensionality of the flow and the decrease of its coherence has permitted a substantial reduction of the energy related to the most coherent mode. As a consequence, this leads to a 12%-decrease in the root mean square values of the side load magnitude. These simulations have clarified that DES is able to predict the unsteadiness of afterbody flows. Moreover, because the transonic dynamics of the afterbody configuration usually leads to serious buffeting coupling effects, most of these recent studies concentrate on flows with a free stream Mach number $M_\infty \approx 0.7$. To improve the performance and the reliability of future launch vehicles, it is also important to have full understanding of the afterbody flows in other flow regimes, for example under low speed conditions at $M_\infty \approx 0.2$ and high speed conditions at $M_\infty \approx 6$. Consequently, different generic rocket configurations within subsonic and hypersonic environments are defined in the research frame of the TR40 subdivision B. As an overview, RANS simulations for these configurations, using different turbulence models, have been reported in the preceding annual report from 2009 [2].

Although corresponding numerical work for the hypersonic flow cases has been conducted in the past year as well, this paper concentrates on the investigation of DES at a subsonic free stream Mach number ($M_\infty \approx 0.2$). The paper is organized as follows. Section 2 introduces the chosen test case and the flow conditions. Section 3 describes the numerical setup and computational approaches. The simulations are discussed in Section 4, which includes the DES results of two differently reduced geometries. The physical interpretation of the numerical results is supported by preliminary experimental results from the RWTH Aachen. The lessons learned and final conclusions are drawn in the last section 5.

2. Test case and flow condition

The dimensions of the geometry are chosen to fit into the open test section wind tunnel of the RWTH Aachen as described by Wolf [6]. The test case is designed to represent a simplified generic launcher configuration. The configuration consists of a blunted cone with a nose radius of 10 mm and an apex angle of 36° followed by a cylinder with a diameter D of 108 mm. The body length is 1080 mm, providing an aspect ratio of 10. The sting support is shaped by an unswept NACA0015 profile, which was supposed to alleviate the wake of the support and minimize the undesirable interaction with the base flow at a distance of 460 mm (≈ 4D) from the airfoil-trailing edge.

The configuration is placed in a flow with a free stream Mach number of 0.2. The main flow parameters of the experiments are summarized in Tab. 1. As shown in the table, all CFD calculations are based on the free stream pressure data of 10^5 Pa. It is difficult, however, to provide an exact value of the free stream pressure in the experiments, since the experiments have been conducted in the open test section of a closed-circuit wind

tunnel. Influences of different experimental and numerical free stream conditions on the simulations will need further investigation.

3. Numerical Setup

3.1. *Numerical method*

The numerical flow field analysis for this study is performed with TAU [7], a DLR flow solver for the compressible Navier-Stokes equations. The DLR-TAU-code is a second order finite-volume approach on hybrid structured and unstructured grids [8].

Different numerical schemes like cell-centered with scalar or matrix-dissipation for sub- and transonic flow and AUSMDV for super- and hypersonic flow conditions are implemented. Second-order accuracy for the upwind schemes is obtained by the MUSCL extrapolation. A three-stage explicit Runge-Kutta scheme as well as an implicit LUSGS scheme are options to advance the solutions in time for steady flow fields. For convergence acceleration local time stepping, implicit residual smoothing and multigrid are implemented.

Fast and accurate transient flow simulations are computed by a second order Jameson type dual time stepping scheme. As an implicit algorithm it is not restricted in the choice of the smallest time step in the flow field. Several one- and two equation turbulence models are available for steady as well as unsteady simulations. In this study the one-equation Spalart-Allmaras (SA) model [9] is used as a baseline model for the DES calculations. The model defines the eddy viscosity field μ_t as

$$\mu_t = \rho\nu_t = \rho\tilde{\nu}f_{\nu 1} \tag{3.1}$$

with the wall function $f_{\nu 1}$ defining the transport quantity $\tilde{\nu}$. The distribution of this transport quantity is determined by the solution of

$$\frac{D(\rho\tilde{\nu})}{Dt} = \underbrace{c_{b1}\tilde{S}\rho\tilde{\nu}}_{P} - \underbrace{c_{w1}f_w\rho\left(\frac{\tilde{\nu}}{d}\right)2}_{D} + \underbrace{\frac{\rho}{\sigma}\left\{\nabla\left[(\nu+\tilde{\nu})\nabla\tilde{\nu}\right] + c_{b2}(\nabla\tilde{\nu})2\right\}}_{DF} \tag{3.2}$$

with d as the wall distance, $\tilde{S}$ as a modified vorticity and an auxiliary function for near wall behavior f_w. The transport equation contains phenomenological models for the diffusion DF, production P, and the destruction term D, of which the last is needed to model the behaviour of the turbulent boundary layer near walls.

During the last decade more advanced turbulence models like DES are implemented [10]. DES is a hybrid RANS-LES approach that is based on a modification of the wall distance term in the SA model. While RANS is used in the unsteady boundary layer flow with a standard grid resolution where it predicts reasonable results, LES is used in separated regions where relevant turbulent scales can be resolved. The switching between RANS and LES is based on a characteristic length scale, chosen to be proportional to Δ which is the largest cell dimension:

$$\Delta = max(\Delta x, \Delta y, \Delta z) \tag{3.3}$$

For the standard DES formulation the wall distance d in the SA model is replaced by $\tilde{d}$ which is defined as:

$$\tilde{d} = min(d, C_{DES}\Delta) \tag{3.4}$$

where C_{DES} is a constant which is calibrated by using isotropic turbulence. Outside of

the boundary layer a local equilibrium between production and destruction terms in the SA model is expected. This local balance leads to the relation $\tilde{\nu} \propto \tilde{S} \cdot \tilde{d}^2$ which is similar to the relation in the Smagorinsky model, namely $\nu_t \propto S \cdot d^2$. Additional features like delayed DES (DDES) that prevents the model from generating unphysical separations by switching into the LES mode too early and low Reynolds number correction for the LES treatment of free shear layers are also available in TAU, as well as the IDDES formulation of Strelets [11].

3.2. *Indicator for assessing the grid resolution quality of a DES*

The spatial discretization error has a large impact on the quality of DES as well as LES results. It is difficult to know a priori what grid spacing is necessary and sufficient to resolve the turbulent structures in detached flow regions, such as free shear layers and separated flow. To overcome this difficulty, Knopp et al. suggest an a posteriori indicator for subsequent grid adaptation. The indicator is based on the resolved turbulent kinetic energy which measures the resolution quality of the LES in such flow regions [12]. The concept of the sensor is to measure the turbulence resolution by the fraction of the resolved to total turbulent kinetic energy.

For statistically steady flow, the following sensor was proposed,

$$I(\overrightarrow{x}) = \frac{k}{k + k_{sgs}}, k = \frac{1}{2} < (\overrightarrow{u} - < \overrightarrow{u} >)^2 >, k_{sgs} = \frac{1}{2} < (\overrightarrow{u} - \overline{\overrightarrow{u}}))^2 > \tag{3.5}$$

where $< . >$ denotes the filtering operator in homogeneous directions and in time and $\overline{\overrightarrow{u}}$ is defined by the convolution integral,

$$\overline{\overrightarrow{u}}(x,t) = \int_{\mathcal{R}} g(\overrightarrow{x} - \overrightarrow{y})\overrightarrow{u}(\overrightarrow{y},t)d\overrightarrow{y} \tag{3.6}$$

with g being the top hat filter function.

Since the turbulent kinetic energy in the residual or subgrid scale motion cannot be computed from resolved quantities it requires a modeling. The underlying idea of $\overrightarrow{u}_{sgs}(\overrightarrow{x},t) \approx \overrightarrow{u}(\overrightarrow{x},t) - \overline{\overrightarrow{u}}(\overrightarrow{x},t)$ is to use a scale similarity assumption for the subgrid scale velocity and then calculate the k_{sgs} by this approach.

The sensor I is designed to stay in a range of [0,1]. Larger values of I mean that larger turbulent fractions are resolved, in comparison with the fraction described by the subgrid model. In the original paper [12], this sensor is designed for automatic grid adaptation, and a value of I above 0.9 is taken as indication for a sufficiently fine grid. More details can be found in Ref. [12].

3.3. *Simulation Strategy*

Being dedicated to engineering applicability the fastest method still capturing the significant flow physics is pursued in this project. Within the huge gap of computational costs for steady RANS calculations and LES, unsteady RANS calculations and DES are available. Unsteady RANS is only useful when the turbulent time scales do not interfere with the time scales of the investigated unsteadiness. Therefore, DES is the method of choice for the study of the base flow field.

The computational expense of a DES scales with the number of points, the numerical effort per point for each unsteady time step and with the spatial (wave numbers) and temporal (statistical error) resolution. As a preliminary study two reduced cases are

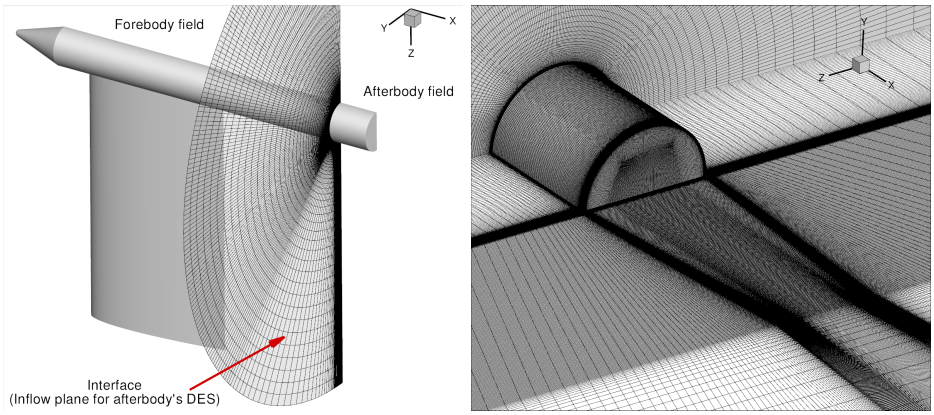

(a) Flow field splitting plane (b) Afterbody part of half body grid

FIGURE 1. Grids generated for the DES of the launch vehicle base flow, 10 million for the half body and 6 million for the half afterbody part

investigated, a split into a forebody and afterbody grid as well as a half body grid utilizing the symmetry of the geometry. In comparison with the future investigation of a full body grid the accuracy and efficiency of these reductions will be evaluated. The current benefit of both DES is the efficient first insight into the unsteady flow physics and the evaluation of the mesh quality according to the above described indicator and the resolution of the instabilities. Beside the a posteriori judgment about the spatial resolution of the conducted DES the indicator will provide hints for an optimized grid to be used for a full body DES.

The splitting of the flow field into forebody and afterbody is motivated from the experience in transonic and supersonic test cases [3], [4], [13]. The flow around the forebody is well captured by a RANS calculation, except perhaps an unsteady behavior in the wake of the model support which is surrounded by a thin shear layer. The intention of the experimental design is to reduce the influence of the support on the base flow as far as possible. Therefore, a well resolved DES of the base flow (afterbody) with constant mean profiles of the incoming turbulent boundary layer would correspond to the idealized experiment. In a subsonic flow field it is generally not a well posed problem to prescribe all flow variables on an inflow plane. Nevertheless, prescribing the exact numerical solution can finally converge to the correct flow field. In default of a sophisticated subsonic near field inflow condition taking even the gap between steady mean profiles and unsteady DES into account, a simple Dirichlet condition is applied for the afterbody simulation. Most of the variables got from the steady RANS calculation, such as the pressure, density, velocity components and SA viscositywill be transferred to initiate the DES calculation.

The half body simulation avoids the problem with the inflow plane and allows interference between the forebody and afterbody flow fields, but it suppresses all non-symmetric behavior over the symmetry plane.

3.4. *Grids*

When generating meshes for DES, particular attention must be taken since the mesh distribution not only controls the accuracy of the RANS solution, but also the resolution of the wavelength spectrum in the LES region. The x-axis is assigned to the cylinder

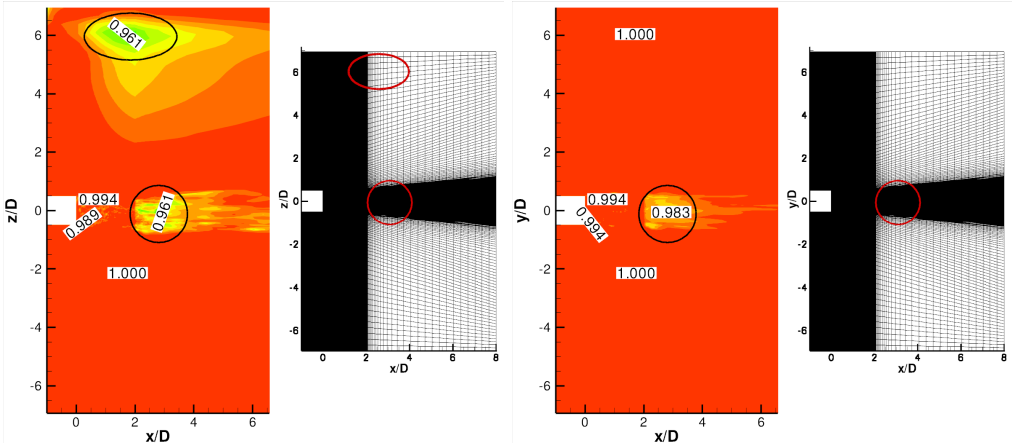

(a) x-z plane (b) x-y plane

FIGURE 2. Contours of the indicator (Eq. 3.5) showing the resolution quality of the afterbody DES

axis with the origin in the base plane and the positive direction on the side of the wake. The z-axis is parallel to the trailing edge of the support, so that the x- and z-axis span the symmetry plane of the geometry. Fig. 1(a) shows the splitting of the flow field into forebody and afterbody parts and the discretization in the interface plane at x = -D. Structured meshes are generated for both parts of the flow d. In the boundary layer regions attached to the body, the y^+ value of the first layer is everywhere below 3, which satisfies the requirements of the RANS part (SA model). Downstream the rear-body, a new grid block is integrated in the center of the base plane to avoid a singularity problem near the x-axis.

The region of main interest is the base flow including the shear layer characteristics and the details of the separation. Therefore, a relatively high grid density is provided at the beginning of the separation where the shear layer is very thin. Special care is taken on the cell isotropy in the separated area ($x < 2D$). In x-direction the length scale is kept in the range of 0.01D. In the azimuthal direction, the base flow field is discretized with 360 points, keeping the edge length in every direction smaller than 0.01D. The number of cells in the afterbody grid is approx. 12 million.

For the half body configuration, the rear part of the grid is similar to the afterbody grid described above and is shown in Fig. 1(b). In the forebody part the cells have been clustered in the wake of the support, as visible in the interface plane of Fig. 1(a). The intention of the clustering is to capture possible vortices in the wake of the support. A geometric stretching technique is used for the radial grid spacing to reduce the number of cells. The stretching ratio leads to a coarser mesh distribution far downstream of the cylinder, which will lower the resolution of turbulent structures in this region. The number of cells for the DES of the half body is in the range of 10 million.

4. Results and Discussion

4.1. *Spatial resolution quality of conducted DES*

During both DES runs the above mentioned indicator gathers the necessary information for the a posteriori discussion of the spatial resolution quality.

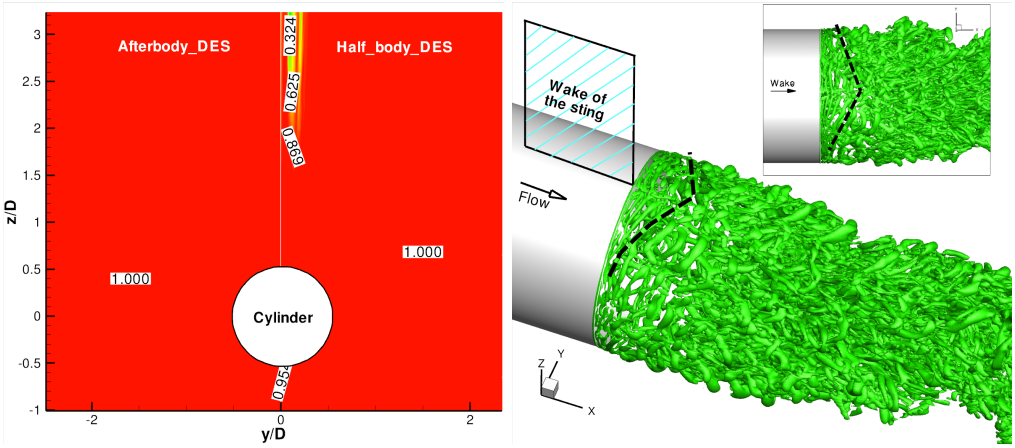

(a) Comparison of the indicator (Eq. 3.5) for the afterbody and half body DES

(b) Iso-surface of Q criterion showing the coherent structures

FIGURE 3. DES indicator and Q criterion in a snapshot of the afterbody DES

Fig. 2(a) and (b) show contour plots of the sensor I for the afterbody DES in the x-z plane and x-y plane respectively. The values of I are above 0.95 all over the field, indicating that the mesh distribution is fine enough to resolve the main turbulent structures in both planes. In the region of interest, the base flow area, I is larger than 0.98, which supports the assumption that the DES has reached a good resolution quality and most of the turbulence structures have been resolved. Two spots with lower I values can be seen in Fig. 2(a). One spot is located in the upper part of the symmetry plane (marked by an ellipse), while the other one is downstream of the base flow (marked by a circle).

There are some common characteristics of these two spots. First of all, both are in the wake of an upstream body. The elliptical zone lies in the wake of the support, and the circular zone is affected by the wake of the base. In the elliptical region, the grid spacing in z-direction reaches the largest value in the field due to the geometric stretching. In the circular zone, the grid spacing in x-direction starts to increase behind the better resolved base flow area. The combination of these two aspects produces zones of relatively low I values. This explains why in the similar discretized x-y plane (Fig. 2(b)) only the circular spot in the base wake is present. The support wake does not influence the x-y plane.

In Fig. 3(a) the DES indicator values in a y-z plane are compared between the afterbody and the half body DES. Although the grid spacing in both cases is quite similar, the half body DES depicted in the right half of the picture receives a much lower indicator value (about 0.32) in the wake region of the support. The grid clustering, which is sufficient to resolve the RANS influence of the support wake, is not able to cover the unsteady support wake in the half body DES. This indicates that mirroring the half body grid will probably be insufficient for a well resolved full body DES.

4.2. *Afterbody DES*

The instantaneous DES flow field is usually presented by showing the iso-surfaces of a positive value of the Q criterion. The Q quantity is the second invariant of the velocity gradient tensor defining vortex tubes as follows,

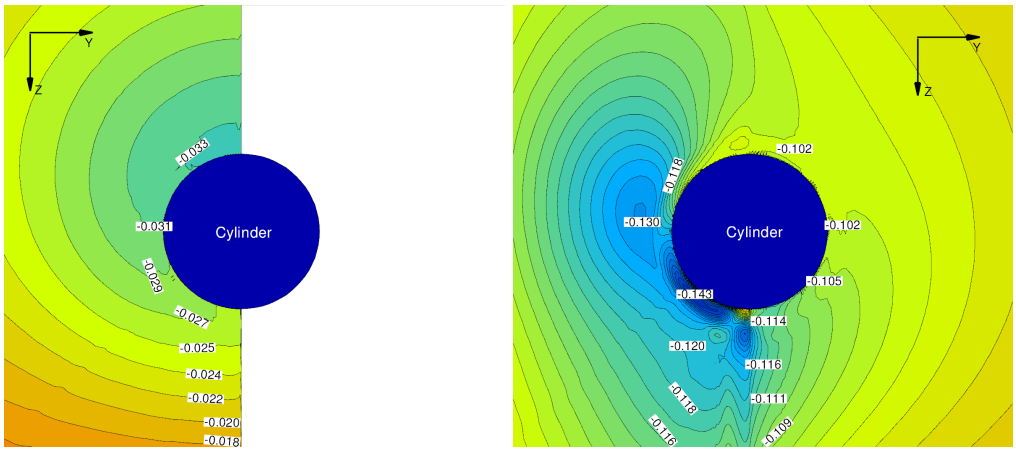

(a) RANS calculation (b) Afterbody DES

FIGURE 4. Comparison of pressure between the RANS calculation and the afterbody DES

$$Q = \frac{1}{2}(\Omega_{ij}\Omega_{ij} - S_{ij}S_{ij}) = -\frac{1}{2}\frac{\partial u_i}{\partial x_j}\frac{\partial u_j}{\partial x_i} > 0 \tag{4.1}$$

where S_{ij} and Ω_{ij} are respectively the symmetric and antisymmetric components of ∇u. In practice finite absolute values of Q are taken to visualize turbulent structures in an instantaneous flow field of a DES.

Most of the turbulent structures in the model wake can be seen in Fig. 3(b). The developing process of the main turbulent structures will be summarized in the following. In the near wake of the separation edge, the roll-up of azimuthal vortical structures apparently occurs. As such structures move downstream, they grow by pairing and will rapidly collapse into large three-dimensional structures.

As a main flow phenomenon of afterbody flows, the generation, development and decay of the shear layer is an important part of LES and DES studies. The afterbody DES shows that the generation of the shear layer is dependent on the azimuthal position. It is visible in Fig. 3(b), that the rate of roll-up of turbulent structures varies behind the base. For instance, downstream of the support wake ($y = 0$, $z = 0.5D$), the turbulence structure has a larger roll-up speed, resulting in a triangular shaped azimuthal turbulence tube behind the cylinder base, as shown in the top-right picture of Fig. 3(b). It indicates that the wake of the sting influences the turbulent structures of the base wake.

Time averaged data are important to study the aerodynamic characteristics of the base flow. For such highly unsteady flow fields, a good time averaged result requires a long time simulation. The DES has progressed to a physical time of some 10 ms, corresponding to a dimensionless time of 200, and will be continued. Such a dimensionless time is known to be too short for the averaged data in the base flow region and therefore those averaged results will be discussed in future studies. Nevertheless, near the inflow boundary the averaged data should be sufficient to test the assumptions made on the flow field by using the Dirichlet condition. The pressure field from the RANS calculation, which is prescribed on the Dirichlet inflow, is compared in Fig. 4 with the time-averaged DES pressure distribution at this boundary.

Two important observations can be extracted from this comparison. At first, the pressure levels of the time averaged DES results differ qualitatively and quantitatively from

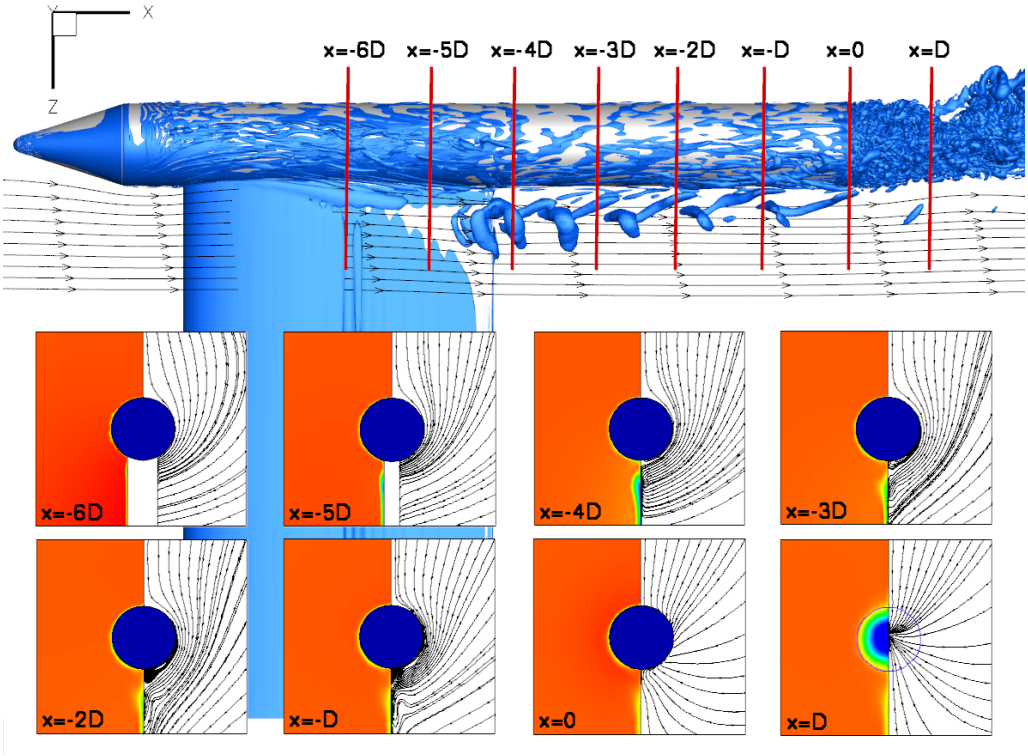

FIGURE 5. Snapshot of an iso-surface of the Q criterion and the time-averaged velocity field in different x-slices. Color contours are used for the x-component (left) and streamlines are plotted of the y- and z-components in each plane (right)

the prescribed RANS data. Secondly, the time-averaged DES pressure is completely non-symmetrical even though the RANS pressure input is perfectly symmetric. This indicates that the simple application of the Dirichlet condition is not sufficient as an inflow condition for the DES in the subsonic case.

4.3. *Half Body DES*

The half body DES has been started later than the afterbody DES and has therefore not yet reached a dimensionless time to discuss the averaged values and statistics of the base wake flow region. In Fig. 5 turbulent structures are visible in the instantaneous iso-surfaces of the Q criterion. Especially interesting are turbulent structures developing in the outer boundary layer of the support towards the base flow region. At the end, they mix with the structures in the base flow. If further statistical analysis will show that an unsteady disturbance from the support wake is influencing the base flow, it would contradict the idealized model assumption of a steady turbulent boundary layer separating at the base. And it is surprising that some vortical turbulence structures emerge on the surface of the main body. According to the concept of DES, in this region an attached boundary layer should be predicted by the RANS mode. The reason for this is still under investigation.

The time-averaged x-velocity contours and streamlines of the time-averaged y- and z-velocities in the respective y-z planes for different x-positions are also shown in Fig. 5. In

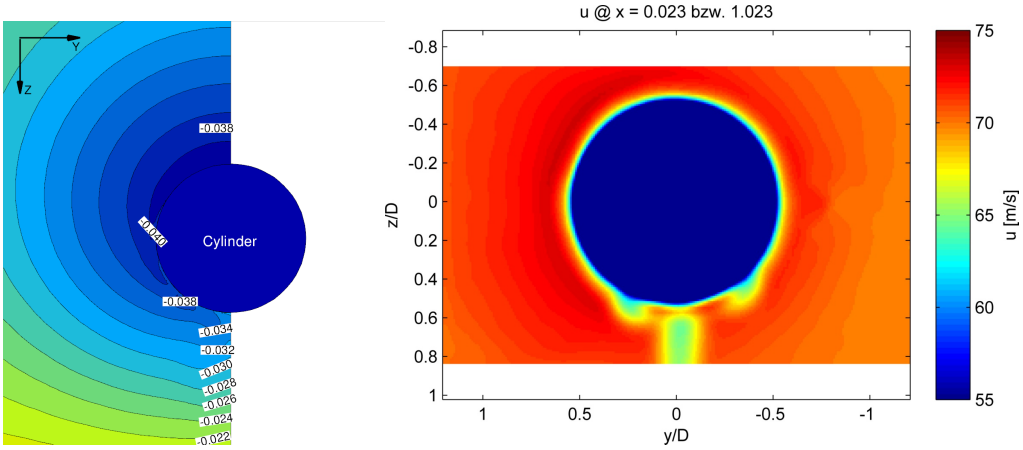

(a) Averaged pressure distribution (b) Experimental x-velocity

FIGURE 6. Averaged pressure distribution at $x = -D$ plane of the half body DES and experimental x-velocity distribution

the time-averaged streamlines of the y-z-velocities the typical vortices generated behind the support and present till the end of the cylinder are visible. It is important not to mismatch these averaged vortices with the turbulent structures mentioned before. The x-velocity contour plots show that the interaction of the airfoil shaped support and the cylinder generates an acceleration of the averaged cylinder boundary layer in the wake of the support as well as an acceleration of the support wake near the cylinder. This observation correlates well with the experimental results, shown in Fig. 6(b).

Fig. 6(a) depicts the time-averaged pressure distribution in the inflow plane of the afterbody DES. Compared with the RANS input data in Fig. 4(a), the pressure distribution from the half body DES looks quite similar, although the pressure levels are slightly lower. Considering the differences between a RANS calculation and a DES, this slight pressure difference seems acceptable.

Returning to an instantaneous flow field, the iso-surfaces of vorticity in the symmetry plane of the half model are shown in Fig. 7. In addition the boundary layer profiles on both sides of the cylinder are schematically depicted. The velocity profile in the wake of the support ($z = 0.5D$) is fuller than on the other side ($z = -0.5D$), although the boundary layer edge velocity is smaller due to the wake. This difference results in some changes of the shear layer properties. On the side of the support wake ($z = 0.5D$) a continuous turbulent shear layer is found, while on the other side a vortex-shedding-like phenomena takes place. It is mainly due to the different developing rates of a shear layer instability.

The boundary layer velocity profiles can also help to explain the appearance of the azimuthal turbulence tube in Fig. 3(b), which has a faster speed downstream of the support wake. Because it is the velocity profile inside the boundary layer which controls the roll-up of the turbulence structures rather than the main velocity outside of the boundary layer, it is believed that the wake of the sting increases the downstream local turbulence intensity and therefore affects the behavior of the shear layer.

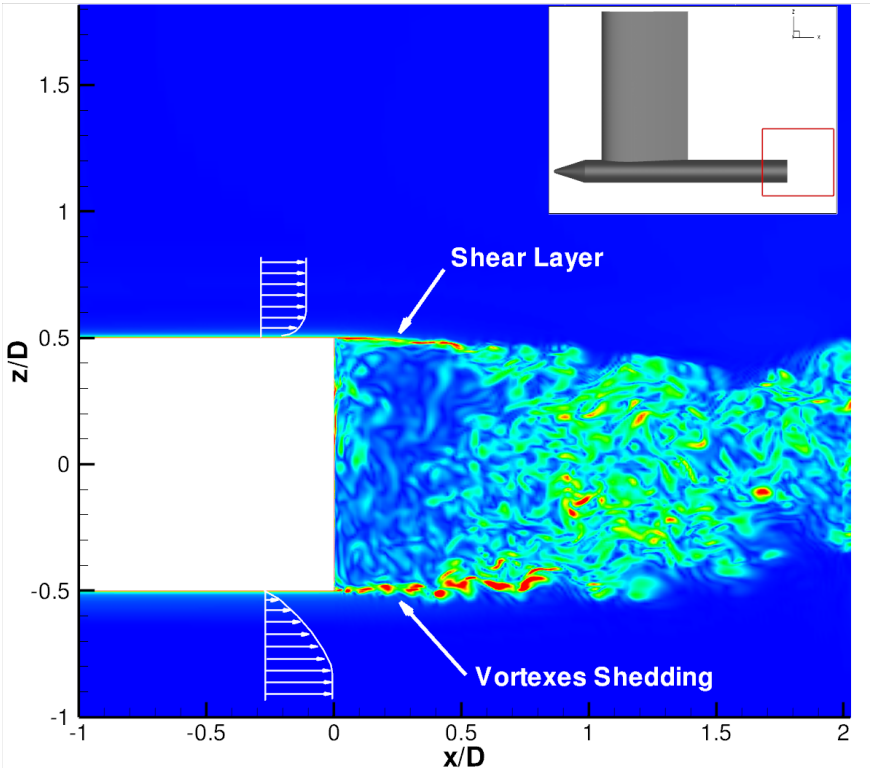

FIGURE 7. Iso-surface of vorticity showing the shear layer

5. Conclusions and Beyond

In the framework of SFB TR40B, the subsonic base flow of a generic rocket model has been investigated. A DES sensor is introduced into the current calculations to check a posteriori whether the grid resolution is good enough to resolve most of the turbulence in the DES. The sensor shows a sufficient grid quality in the base flow region for both DES conducted for reduced geometric complexity. Furthermore, the sensor highlights regions where the grid for a future full body DES could be improved compared to the meshes used in this preliminary study.

The simple Dirichlet inflow condition for the afterbody DES is found to be not suitable for the investigated geometry at low Mach number flows due to interactions of turbulent structures from the support with the shear layer of the base flow.

Both DES show an azimuthal dependency of the turbulent structures in the instantaneous shear layer around the base, but are not yet progressed far enough to discuss the averaged and especially the statistical values of the base flow in detail. The half body DES indicates a link between the wake of the support and the wake of the base, which will be investigated further in the succeeding DES around the full geometry.

Acknowledgments

Financial support has been provided by the German Research Council (Deutsche Forschungsgemeinschaft - DFG) in the framework of the Sonderforschungsbereich Transregio 40.

References

[1] LÜDEKE, H., CALVO, J.B. AND FILIMON, A. (2006). Fluid Structure Interaction at the Ariane 5 Nozzle Section by advanced Turbulence Models. *Proceedings of the European Conference on Computational Fluid Dynamics ECCOMAS CFD*, Egmond aan zee, NL.

[2] BUANGA, B., HANNEMANN, V., LÜDEKE, H. AND YOU, Y. (2009). Modeling of the interaction between a space vehicle's external flow and its plume. *Sonderforschungsbereich/Transregio40 - Annual Report 2009*

[3] LÜDEKE, H. (2005). Investigation of the Ariane 5 Nozzle Section by DES. *6th International Symposium on Launcher Technologies*, Munich, Germany.

[4] DECK, S. AND ERIK G. (2004). Detached and Large Eddy Simulation of Unsteady Side-Loads Over An Axisymmetric Afterbody. *Proceedings of the Fifth European Symposium on Aerothermodynamics for Space Vehicles*, Cologne, Germany.

[5] WEISS, P.E., DECK, S. AND SAGAUT, P. (2010). On the Control of Turbulent Axisymmetric Separating/Reattaching Flows Using Zonal Detached Eddy Simulation. *AIAA 2010-5087*.

[6] WOLF, C. AND HENKE, R. (2009). Base-flow investigation of a generic rocket configuration in subsonic free stream conditions. *Sonderforschungsbereich/Transregio 40 - Annual Report 2009*

[7] MACK, A. AND HANNEMANN, V. (2002). Validation of the unstructured DLR-TAU Code for Hypersonic Flows. *AIAA 2002-3111*.

[8] REIMANN, B., JOHNSTON, I. AND HANNEMANN, V. (2004). DLR-TAU Code for High Enthalpy Flows. *Notes on Numerical Fluid Mechanics and Multidisciplinary Design*, **87**, 99–106, Springer DE.

[9] SPALART, P.R., JOU, W.H., STRELETS, M. AND ALLMARAS, S.R. (1997). Comments on the feasibility of LES for wings, and on a hybrid RANS/LES approach. *Advances in DNS/LES*, 137–147, Greyden Press.

[10] SPALART, P.R. (2001). Young-Person's Guide to Detached- Eddy Simulation Grids. *NASA/CR-2001-211032.*

[11] TRAVIN, A.K., SHUR, M.L., SPALART, P.R. AND STRELETS, M.KH. (2006). Improvement of Delayed Detached Eddy Simulation for LES With Wall Modelling. *ECCOMAS CFD 2006*.

[12] KNOPP, T., ZHANG, X., KESSLER, R., AND LUBE, G. (2010). Enhancement of an industrial finite-volume code for large-eddy-type simulation of incompressible high Reynolds number flow using near-wall modeling. *Comput. Methods Appl. Mech. Energ.*,**227**, 890-902.

[13] FILIMON, A. (2006). Transsonischer Zylindernachlauf unter Einfluss eines Düsenstrahls und Untersuchung der Turbulenz-Stoß-Interaktion. *Diplomarbeit am Institut für Aerodynamik und Gasdynamik der Uni Stuttgart*.